Electronic Supplementary Material (ESI) for Journal of Materials Chemistry A.


Supporting Information

# A new dual-ion hybrid energy storage system with energy density comparable to ternary lithium ion batteries

Shenggong He[1†], Shaofeng Wang[1], Hedong Chen[1†], Xianhua Hou[1*], and Zongping Shao[2,3*]

[1]Guangdong Provincial Key Laboratory of Quantum Engineering and Quantum Materials, Guangdong Engineering Technology Research Center of Efficient Green Energy and Environment Protection Materials, Engineering Research Center of MTEES (Ministry of Education), School of Physics and Telecommunication Engineering, South China Normal University, Guangzhou 510006, China;

[2]Jiangsu National Synergetic Innovation Center for Advanced Materials (SICAM), State Key Laboratory of Materials-Oriented Chemical Engineering, College of Chemical Engineering, Nanjing Tech University, Nanjing, 210009, china;

[3]WA School of Mines: Minerals, Energy and Chemical Engineering (WASM-MECE), Curtin University, Perth, WA, 6845 Australia;

E-mail: *houxianhua@m.scnu.edu.cn (X.H. Hou); Shaozp@njtech.edu.cn (Z.P. Shao)*

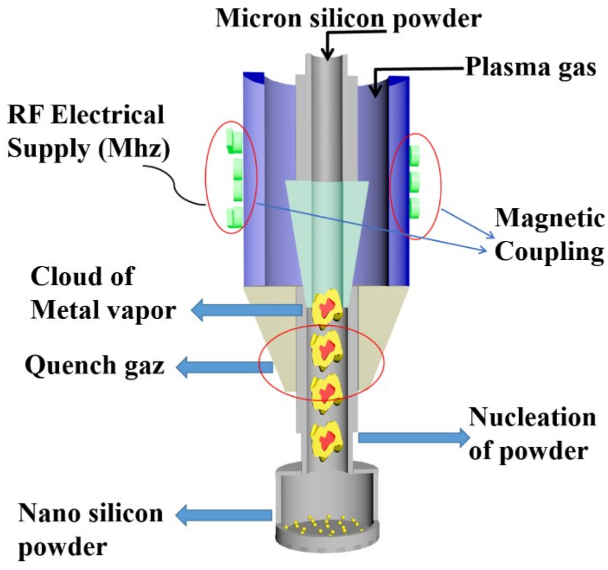


**Scheme 1.** Synthesis of nano silicon by radio frequency induction plasma technology.

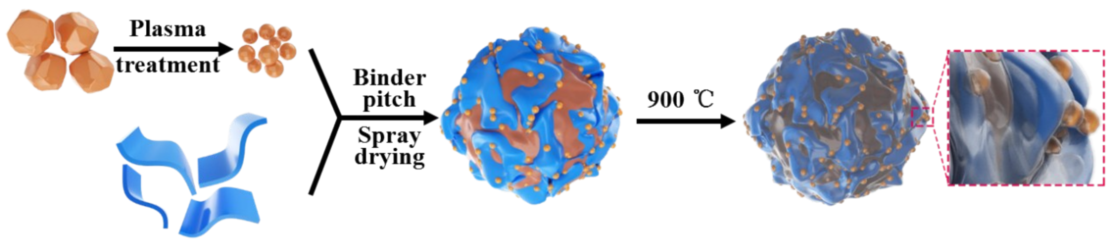


**Scheme 2.** Graphic diagram of the synthesis process for Si/C composite.

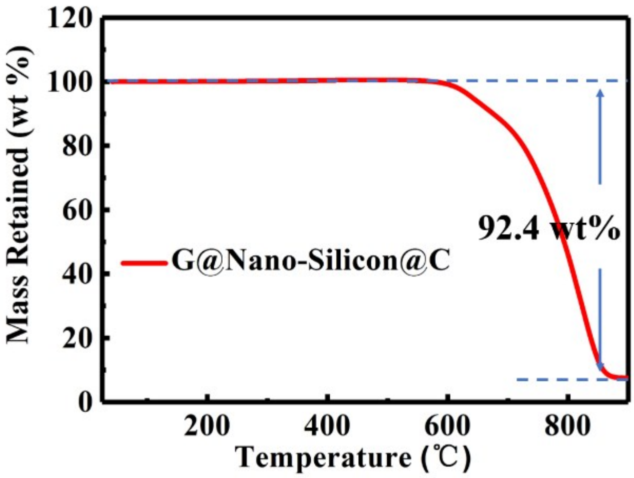


**Figure S1.** TG profiles of Si/C.

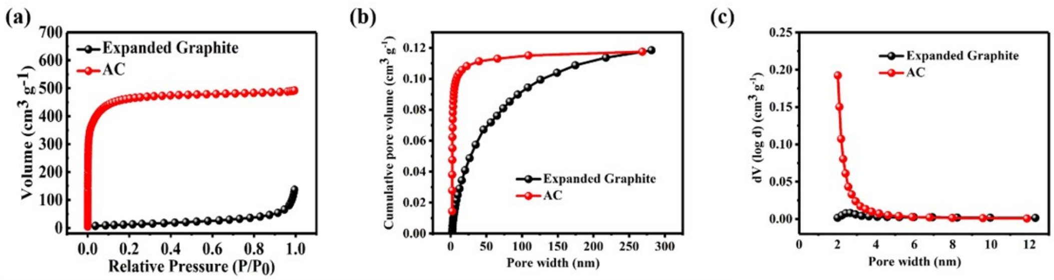


**Figure S2.** (a) EG and AC samples show two different type of nitrogen absorption-desorption isotherms, suggesting plate-like structure of EG and macroporous channels of AC, and the BET surface area are 90.2 $m^2$ $g^{-1}$ and 1768 $m^2$ $g^{-1}$, respectively. (b,c) The pore volume of EG and AC is 0.110 and 0.761 $cm^3$ $g^{-1}$, respectively.

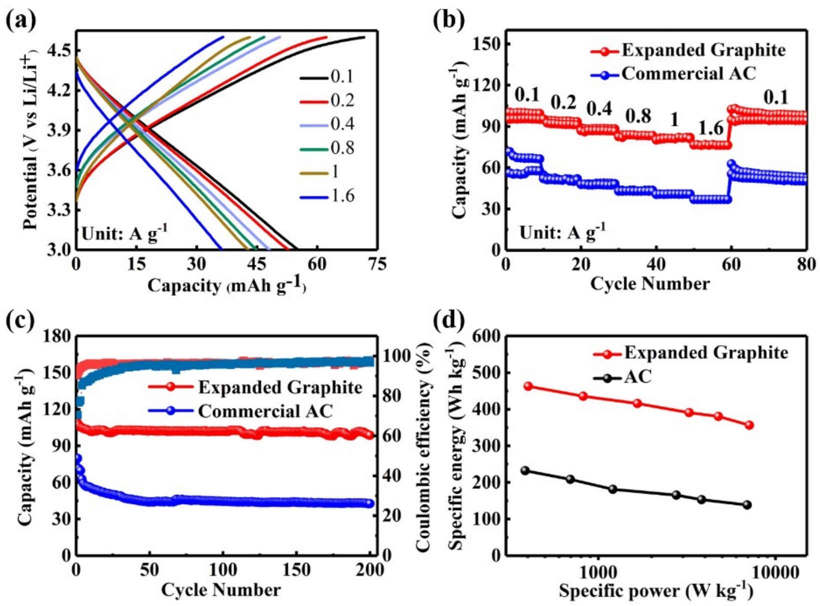


**Figure S3.** (a) Charge-discharge curves of AC cathode at 3-4.6 V under different current rates. (b) Rate performance for the EG and AC cathode. (c) The long-term cycling performance of the EG and AC cathode at 100 mA $g^{-1}$. d) Ragone plots of EG and AC cathodes normalized by the mass of cathode.

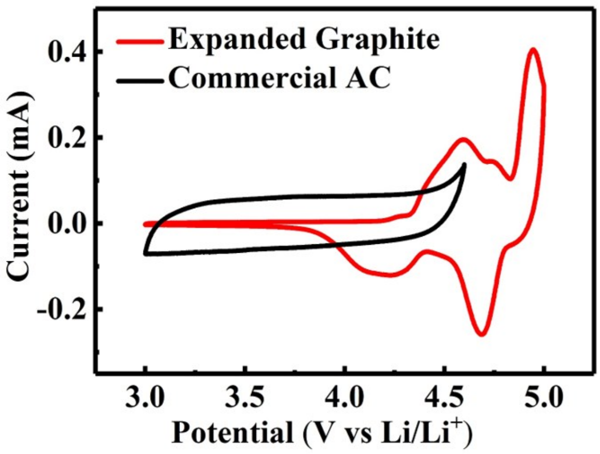


**Figure S4.** Electrochemical characterization of EG and AC cathode, CV curves for AC and EG cathode at 0.8 mV $s^{-1}$.

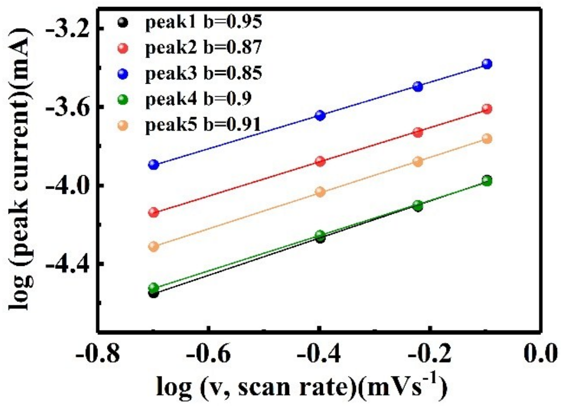


**Figure S5.** Log(i) vs log(v) plots to determine the value of each redox peak for EG cathode.

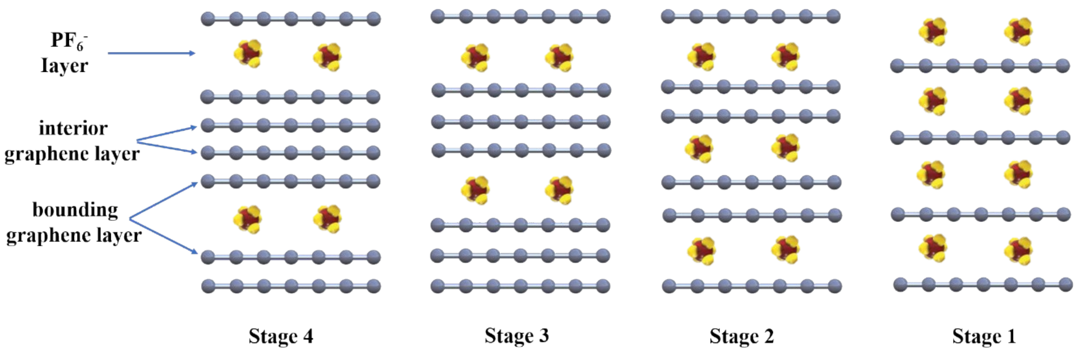


**Figure S6.** Schematic illustration for various stages of EG intercalation compounds.

**Note S1: Energy density and power density calculation of EG and AC cathodes.**

The specific energy ($E_{cathode}$; Wh/kg) of cathode was calculated by $\mathbf{E_{cathode} = C_{cathode} * V_m}$; $C_{cathode}$ (mAh/g) is the discharge capacity of cathode in half cell at various current densities, and $V_m$ (V) is the midpoint discharge voltage obtained from the discharge curves.

The specific power ($P_{cathode}$; W/kg) of cathode can be estimated as

$\mathbf{P_{cathode} = E_{cathode} / t}$; t is the discharging time (h).

**Table S1.** Energy and power density of EG cathodes.

| **Current density ($A\ g^{-1}$)** | **0.1** | **0.2** | **0.4** | **0.8** | **1** | **1.6** |
|---|---|---|---|---|---|---|
| **$C_{EG}$ ($mAh\ g^{-1}$)** | **101.3** | **95.1** | **89.0** | **83.8** | **81.7** | **76.5** |
| **Energy density ($W\ kg^{-1}$)** | **462.9** | **435.5** | **415.7** | **390.9** | **380.7** | **356.5** |
| **Power density ($Wh\ kg^{-1}$)** | **403** | **822** | **1663** | **3257** | **4759** | **7130** |

**Table S2.** Energy and power density of AC cathodes.

| Current density ($A\ g^{-1}$) | 0.1 | 0.2 | 0.4 | 0.8 | 1 | 1.6 |
|---|---|---|---|---|---|---|
| $C_{AC}$ ($mAh\ g^{-1}$) | 60.9 | 54.7 | 48.0 | 43.6 | 40.7 | 36.9 |
| Energy density ($W\ kg^{-1}$) | 232.2 | 208.4 | 181.4 | 165.5 | 153.1 | 138.5 |
| Power density ($Wh\ kg^{-1}$) | 387 | 695 | 1209 | 2758 | 3826 | 6925 |

**Note S2: Energy density and power density calculation of dual-ion hybird devices (Si/C//EG).**

The discharge capacity $\mathbf{C_{cathode}}$ (based on EG mass in cathode) and $V_m$ of dual-ion hybird devices (Si/C//EG) can be obtained from the discharge curves at different current rates. The cell capacity can be obtained by

$\mathbf{C_{ell} = C_{cathode} \times m_{cathode} / (m_{cathode} + m_{anode} + m_{electrolyte})}$.

The energy density of full cells can be simplified as

$\mathbf{E_{cell} = C_{ell} \times V_m}$;

The power density of the full cells can be estimated as

$\mathbf{P_{cell} = E_{cell} / t}$; **t** is the discharging time (h).

**Table S3.** Energy and power density of dual-ion hybird devices (Si/C//EG).

| **Current density ($A\ g^{-1}$)** | **0.1** | **0.2** | **0.4** | **0.8** | **1** | **1.6** |
|---|---|---|---|---|---|---|
| **$C_{EG}$ ($mAh\ g^{-1}$)** | **109.8** | **106.6** | **101.7** | **96.4** | **93.2** | **88.9** |
| **$C_{LDIpC}$ ($mAh\ g^{-1}$)** | **60.2** | **58.5** | **55.8** | **52.9** | **51.1** | **48.8** |
| **Energy density ($W\ kg^{-1}$)** | **252.0** | **244.6** | **234.5** | **231.3** | **228.9** | **222.6** |
| **Power density ($Wh\ kg^{-1}$)** | **215** | **445** | **938** | **1928** | **2861** | **5420** |

**Table S4.** Comparison of the electrochemical properties between the present dual-ion hybrid devices (Si/C//EG) and previously SCs, LICs, pseudocapacitors and DIB.

| **Materials (anode//cathode)** | **Voltage Window (V)** | **Energy density** | **Power density** | **Cycling stability** | **Ref.** |
|---|---|---|---|---|---|
| Ni-MDH//N-C | 0.0-1.7 | 81 Wh $kg^{-1}$ | 1900 W $kg^{-1}$ | 91.3%, 10000 cycles | **1** |
| MoPO/EG//$MnO_x$/EG | 0.0-2.7 | 89.2 Wh $kg^{-1}$ | 2733 W $kg^{-1}$ | Nearly no fading 100000 cycles | **2** |
| $NiCo_2Al$-LDH//ZPC | 0.0-1.5 | 44 Wh $kg^{-1}$ | 462 W $kg^{-1}$ | 91.2%, 15000 cycles | **3** |
| $Fe_3O_4$/RGO//RGO | 1.0-4.0 | 147 Wh $kg^{-1}$ | 150 W $kg^{-1}$ | 70%, 10000 cycles | **4** |
| BNC//BNC | 0.02-4.5 | 220 Wh $kg^{-1}$ | 225 W $kg^{-1}$ | 81%, 5000 cycles | **5** |
| Si/C//RAC | 0.02-4.0 | 227 Wh $kg^{-1}$ | 1146 W $kg^{-1}$ | Nearly no fading 16000 cycles | **6** |
| $Zn_xCo_{1-x}O$// $Zn_xCo_{1-x}O$ | 0.0-1.45 | 67.3 Wh $kg^{-1}$ | 1670 W $kg^{-1}$ | 90.7%, 5000 cycles | **7** |
| VN-RGO//APDC | 0.0-4.0 | 162 Wh $kg^{-1}$ | 200 W $kg^{-1}$ | 83%, 1000 cycles | **8** |
| Al//G | 0.5-2.25 | 40 Wh $kg^{-1}$ | 3000 W $kg^{-1}$ | Nearly no fading 7500 cycles | **9** |
| G//G | 0.0-5.0 | 233 Wh $kg^{-1}$ | 220 W $kg^{-1}$ | 96.1%, 1400 cycles | **10** |
| Si/C//EG | 0.0-5.0 | 252 Wh $kg^{-1}$ | 215 W $kg^{-1}$ | 90.9%, 1000 cycles | **This work** |

**Table S5.** Crystal structure of EG cathodes at different charge states.

| Potential | $2\theta_{(00n)}$/° | $2\theta_{(00n+1)}$/° | n | Stage x | $I_c$/Å | $d_i$/Å | Δd/Å | Δc |
|---|---|---|---|---|---|---|---|---|
| **4.55V** | **25.150** | **30.014** | **5** | **4** | **17.690** | **7.307** | **3.846** | **27.8%** |
| **4.60V** | **24.897** | **31.015** | **4** | **3** | **14.294** | **7.372** | **3.911** | **37.7%** |
| **4.86V** | **24.226** | **32.301** | **3** | **2** | **11.013** | **7.552** | **4.091** | **59.1%** |
| **5.0V** | **23.207** | **34.246** | **2** | **1** | **7.659** | **7.659** | **4.198** | **121.2%** |
| **4.77V** | **24.211** | **32.381** | **3** | **2** | **11.019** | **7.558** | **4.097** | **59.2%** |
| **4.32V** | **24.874** | **30.916** | **4** | **3** | **14.307** | **7.385** | **3.924** | **37.8%** |

$$d_{00n} = \frac{I_c}{n} = \frac{\lambda}{2\sin\theta_{00n}} \quad (1)$$

$$d_{00n+1} = \frac{I_c}{n+1} = \frac{\lambda}{2\sin\theta_{00n+1}} \quad (2)$$

$$n = \frac{1}{\dfrac{\sin\theta_{00n+1}}{\sin\theta_{00n}} - 1} \quad (3)$$

$$x = n - 1 \quad (4)$$

$$I_c = d_i + (x-1) \times 3.461 \quad (5)$$

$$\Delta d = d_i - 3.461 \quad (6)$$

$$\Delta c = \left(\frac{I_c}{x \times 3.461} - 1\right) \times 100\% \quad (7)$$

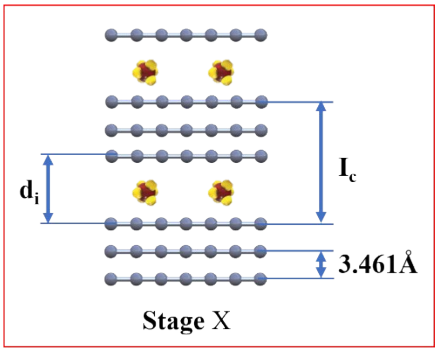


$\mathbf{d_{00n}}$ is the spacing of the (00n) plane, $\mathbf{I_c}$ is periodic repeat distance, **n** is the Miller indices, **λ** is the X-ray wavelength (1.540598 Å); $\boldsymbol{\theta_{00n}}$ and $\boldsymbol{\theta_{00n+1}}$ are the measured Bragg angle of (00n) and (00n+1) peaks, **x** is the Stage integer, $\mathbf{d_i}$ is the intercalant gallery height, Δ**d** is the gallery expansion, Δ**c** is the percent expansion.

## References


1. Qu, C.; Zhao, B.; Jiao, Y.; Chen, D.; Dai, S.; deglee, B. M.; Chen, Y.; Walton, K. S.; Zou, R.; Liu, M., Functionalized Bimetallic Hydroxides Derived from Metal–Organic Frameworks for High-Performance Hybrid Supercapacitor with Exceptional Cycling Stability. *ACS Energy Letters* **2017,** *2* (6), 1263-1269.
2. Song, Y.; Deng, P.; Qin, Z.; Feng, D.; Guo, D.; Sun, X.; Liu, X.-X., A polyanionic molybdenophosphate anode for a 2.7 V aqueous pseudocapacitor. *Nano Energy* **2019,** *65*, 104010.
3. Gao, X.; Liu, X.; Wu, D.; Qian, B.; Kou, Z.; Pan, Z.; Pang, Y.; Miao, L.; Wang, J., Significant Role of Al in Ternary Layered Double Hydroxides for Enhancing Electrochemical Performance of Flexible Asymmetric Supercapacitor. *Advanced Functional Materials* **2019,** *29* (36), 1903879.
4. Zhang, F.; Zhang, T.; Yang, X.; Zhang, L.; Leng, K.; Huang, Y.; Chen, Y., A high-performance supercapacitor-battery hybrid energy storage device based on graphene-enhanced electrode materials with ultrahigh energy density. *Energy & Environmental Science* **2013,** *6* (5), 1623-1632.
5. Xia, Q.; Yang, H.; Wang, M.; Yang, M.; Guo, Q.; Wan, L.; Xia, H.; Yu, Y., High Energy and High Power Lithium-Ion Capacitors Based on Boron and Nitrogen Dual-Doped 3D Carbon Nanofibers as Both Cathode and Anode. *Advanced Energy Materials* **2017,** *7* (22), 1701336.
6. Li, B.; Xiao, Z.; Chen, M.; Huang, Z.; Tie, X.; Zai, J.; Qian, X., Rice husk-derived hybrid lithium-ion capacitors with ultra-high energy. *Journal of Materials Chemistry A* **2017,** *5* (46), 24502-24507.
7. Ling, T.; Da, P.; Zheng, X.; Ge, B.; Hu, Z.; Wu, M.; Du, X. W.; Hu, W. B.; Jaroniec, M.; Qiao, S. Z., Atomic-level structure engineering of metal oxides for high-rate oxygen intercalation pseudocapacitance. *Sci Adv* **2018,** *4* (10), eaau6261.
8. Wang, R.; Lang, J.; Zhang, P.; Lin, Z.; Yan, X., Fast and Large Lithium Storage in 3D Porous VN Nanowires-Graphene Composite as a Superior Anode Toward High-Performance Hybrid Supercapacitors. *Advanced Functional Materials* **2015,** *25* (15), 2270-2278.
9. Lin, M. C.; Gong, M.; Lu, B.; Wu, Y.; Wang, D. Y.; Guan, M.; Angell, M.; Chen, C.; Yang, J.; Hwang, B. J.; Dai, H., An ultrafast rechargeable aluminium-ion battery. *Nature* **2015,** *520* (7547), 325-8.
10. Wang, G.; Oswald, S.; Loffler, M.; Mullen, K.; Feng, X., Beyond Activated Carbon: Graphite-Cathode-Derived Li-Ion Pseudocapacitors with High Energy and High Power Densities. *Adv Mater* **2019,** *31* (14), e1807712.